Synaptic properties of the lemniscal and paralemniscal pathways to the mouse somatosensory thalamus

Christina Mo[a,1], Iraklis Petrof[a,1,2], Angela N. Viaene[a,3], and S. Murray Sherman[a,4]

[a]Department of Neurobiology, University of Chicago, Chicago, IL 60637

Edited by Thomas D. Albright, The Salk Institute for Biological Studies, La Jolla, CA, and approved June 13, 2017 (received for review February 24, 2017)

Somatosensory information is thought to arrive in thalamus through two glutamatergic routes called the lemniscal and paralemniscal pathways via the ventral posterior medial (VPm) and posterior medial (POm) nuclei. Here we challenge the view that these pathways functionally represent parallel information routes. Using electrical stimulation and an optogenetic approach in brain slices from the mouse, we investigated the synaptic properties of the lemniscal and paralemniscal input to VPm and POm. Stimulation of the lemniscal pathway produced class 1, or "driver," responses in VPm relay cells, which is consistent with this being an information-bearing channel. However, stimulation of the paralemniscal pathway produced two distinct types of responses in POm relay cells: class 1 (driver) responses in 29% of the cells, and class 2, or "modulator," responses in the rest. Our data suggest that, unlike the lemniscal pathway, the paralemniscal one is not homogenous and that it is primarily modulatory. This finding requires major rethinking regarding the routes of somatosensory information to cortex and suggests that the paralemniscal route is chiefly involved in modulatory functions rather than simply being an information route parallel to the lemniscal channel.

driver | modulator | glutamatergic | ventral posterior medial nucleus | posterior medial nucleus

Before reaching the cortex, all sensory information except olfaction is relayed by the thalamus. For somatosensory information, there appear to be two potential routes of such information flow, which have been termed "lemniscal" and "paralemniscal." Regarding the trigeminal components of these, the lemniscal route is represented by the pathway from the principal and spinal nuclei of the Vth nerve (PrV and SpV, respectively) via the medial lemniscus (ML) through VPm, whereas the paralemniscal route is represented by the pathway originating mostly from SpV through POm. However, exactly how these circuits function depends critically on the nature of the underlying synapses. These inputs to thalamus and from thalamus to cortex are glutamatergic, meaning that they use glutamate as a neurotransmitter. Recent work has made it clear that glutamatergic inputs in thalamus and cortex are heterogeneous and can be divided into at least two types, known as class 1 (or driver) and class 2 (or modulator) (1–3). It has been suggested that the class 1 inputs carry the main information between neuronal regions and that the class 2 inputs provide a modulatory role, mainly affecting how class 1 inputs are processed (reviewed in refs. 4–6; see also *Discussion*). Thus, identifying which type of glutamatergic synapses are involved in the lemniscal and paralemniscal pathways could help clarify whether they represent parallel information routes or whether some other functional explanation is more plausible.

To this end, we used slice preparations in which we could use a combination of electrical stimulation and optogenetics to activate lemniscal or paralemniscal inputs to patched cells in VPm and POm, respectively. We found that all recorded VPm cells receive a class 1 input activated by stimulation of the ML, whereas a majority of recorded POm cells receive a class 2 input from activation of inputs from SpV, with the remaining minority receiving a class 1 input. The latter finding of mostly class 2 input in the paralemniscal innervation of POm raises questions about its functional role.

Methods

Slice Preparation. BALB/c mice (aged 10–28 d) were anesthetized with a few drops of isoflurane and decapitated. Brains were quickly removed and placed in chilled (0–4 °C), oxygenated (95% O_2, 5% CO_2) slicing solution containing the following (in mM): 2.5 KCl, 1.25 NaH_2PO_4, 10 $MgCl_2$, 0.5 $CaCl_2$, 26 $NaHCO_3$, 11 glucose, and 206 sucrose. We prepared 500 μm-thick lemniscal slices, containing the medial lemniscal axons terminating in VPm, as follows: Brains were blocked at a 20° sagittal angle from the midline, and the blocked side was glued onto a vibratome platform (Leica). The paralemniscal slice, containing the axons of cells originating in SpV and terminating in POm, was prepared by cutting 500 μm-thick slices at a 40–45° angle relative to the horizontal plane. Given that the inclusion of the entire lemniscal or paralemniscal pathway was not possible in either case, both slice preparations were cut with the intention of maximizing the length of the brainstem-originating axons terminating in VPm and POm, respectively. Fibers from layer 5 of S1 terminating in POm collateralize near or at the level of the internal capsule and send branches to the anterior pretectal nucleus (APT) (7) not far from where we would usually place our stimulating electrode to activate the paralemniscal pathway (see *Flavoprotein Autofluorescence Imaging*). As a result, we wanted to minimize the possibility of antidromically activating the corticotectal branch of those fibers, and thus orthodromically activating of their corticothalamic branch terminating in POm. To do so, further cuts were made on paralemniscal slices to remove tissue lateral to the internal capsule and therefore eliminate this region of layer 5 axonal branching from our preparation.

Once cut, slices from either preparation were placed in warm (32 °C) oxygenated ACSF [containing (in mM) 125 NaCl, 3 KCl, 1.25 NaH_2PO_4, 1 $MgCl_2$, 2 $CaCl_2$, 25 $NaHCO_3$, 25 glucose] for 30 min and were then allowed to recover for at least an additional 30 min, at room temperature, before being used. Once in the recording chamber, slices were continuously perfused with oxygenated ACSF.

Significance

Functional mapping of the routes of information processing is essential to understand how the brain operates. The main carriers of information are excitatory (glutamatergic) neurons, which form synapses that can either reliably deliver information or modify it. Using the somatosensory system in the mouse, we show that the two parallel glutamatergic routes from periphery to cortex should not be considered equal in carrying somatosensory information. Instead, one route has synapses solely suited for fast information transfer—the Lemniscal pathway—and the other suited for mainly modifying such information—the Paralemniscal pathway. This is an example of synaptic and anatomical analyses that inform circuit function and build on a framework for feedforward and feedback processing.

Author contributions: C.M., I.P., A.N.V., and S.M.S. designed research; C.M. and I.P. performed research; C.M., I.P., A.N.V., and S.M.S. analyzed data; and C.M., I.P., A.N.V., and S.M.S. wrote the paper.

The authors declare no conflict of interest.

This article is a PNAS Direct Submission.

[1]C.M. and I.P. contributed equally to this work.

[2]Present address: Abramson Research Center, The Children's Hospital of Philadelphia, Philadelphia, PA 19104.

[3]Present address: Division of Neuropathology, Department of Pathology and Laboratory Medicine, Hospital of the University of Pennsylvania, Philadelphia, PA 19104.

[4]To whom correspondence should be addressed. Email: msherman@bsd.uchicago.edu.

Flavoprotein Autofluorescence Imaging. The two slice preparations described above were developed with the use of the flavoprotein autofluorescence (FA) imaging technique (8). FA measures green light (520–560 nm) emitted by mitochondrial flavoproteins under blue light (472–488 nm) in conditions of metabolic activity associated with postsynaptic activation (8, 9). Once a particular area of tissue has been stimulated, FA uses the elevated levels of mitochondrial green light emissions to detect cellular activation in remote areas of the slice, a sign of connectivity. FA was carried out using a QImage Retiga-SRV camera (QImaging Corporation) attached onto a fluorescent light-equipped microscope (Axioscop 2FS, Carl Zeiss Instruments).

The lemniscal pathway was activated through the electrical stimulation of ML fibers, which originate in PrV and were clearly discernable in our visualized slice setup. On the other hand, paralemniscal axons originating in SpV ascend through the brainstem and cross the midline into contralateral POm in bundles that are not clearly visible. To stimulate these fibers in our paralemniscal slice, we placed the stimulating electrode adjacent to the APT or next to, it in the region through which these fibers travel before arriving at POm.

The stimulation protocol for FA imaging trials consisted of current injection trains (10 pulses at 20 Hz and 150–300 μA) delivered through a concentric bipolar electrode (FHC). FA activity was recorded for a total of 14 s, including 1.5 s before stimulation and 12 s following stimulation. FA images were acquired at 2.5–10 frames per second (integration time of 100–400 ms). The final image was generated as a function of the $\Delta f/f$ ratio of the baseline autofluorescence of the slice before stimulation subtracted from the autofluorescence of the slice over the period of stimulation (Δf) divided by baseline (f).

Electrophysiology. Current clamp and voltage clamp mode whole-cell recordings were carried out in a visualized slice setup under a DIC-equipped Axioscop 2FS microscope (Carl Zeiss Instruments) and with a Multiclamp 700B amplifier and pCLAMP software (Axon Instruments). Recording glass pipettes with input resistances of 5–9 MΩ were filled with intracellular solution containing (in mM) 117 K-gluconate, 13 KCl, 1 $MgCl_2$, 0.07 $CaCl_2$, 10 Hepes, 0.1 EGTA, 2 Na_2-ATP, 0.4 Na-GTP, pH 7.3, 290 mosm. Electrical stimulation of the two pathways was delivered through a concentric bipolar electrode, which carries the advantage of delivering a current to a relatively restricted tissue area. Short-term plasticity (paired-pulse depression vs. paired-pulse facilitation) was examined using a stimulation protocol consisting of four 0.1 ms-long pulses at a frequency of 10 Hz. To minimize further the spread of the passed current (which could potentially result in the recruitment of additional afferent pathways of the recorded area), the assessment of paired-pulse effects was carried out for the lowest stimulation intensity capable of inducing excitatory postsynaptic potentials (EPSPs) of an amplitude greater than 0.5 mA (for at least 3 of the 4 EPSPs) in the recorded cells (see *Results*). We calculated the E2/E1 ratio by dividing the amplitude of the second evoked EPSP by the amplitude of the first. An E2/E1 ratio of >1 indicates paired-pulse facilitation, whereas an E2/E1 ratio of <1 indicates paired-pulse depression.

For the assessment of the relationship between the intensity of the injected current and the amplitude of the postsynaptic effects (i.e., all-or-none versus graded response patterns), we applied stimulations of gradually increasing intensity (typically at increments of 50 μA). A high-frequency stimulation protocol (0.1 ms-long pulses delivered at 125 Hz over 200–500 ms, 100–300 μA) was used for the examination of metabotropic glutamate receptor activation.

All experimental protocols, unless stated otherwise, were performed in the presence of $GABA_A$ and $GABA_B$ receptor antagonists (SR95531, 50 nM and CGP46381, 50 nM, respectively). Moreover, NMDA and AMPA receptor antagonists (AP5, 100 μM and DNQX, 50 μM, respectively) were applied during high-frequency stimulation to isolate any metabotropic glutamate responses. Where long-lasting (>1 s) membrane potential changes were seen under these conditions, we were able to block them with bath application of the type 1 metabotropic glutamate receptor antagonist LY367385 (40 μM). All data were digitized on a Digidata 1200 board and stored on a computer. Analyses of the acquired traces were performed in ClampFit (Axon) software.

Injections of AAV and Optogenetic Stimulation. All surgical procedures described here and later were in accordance with the guidelines of the Institutional Animal Care and Use Committee at the University of Chicago. BALB/c mice (age 8–15 d) of both sexes were anesthetized with a ketamine (100 mg/kg)–xylazine (3 mg/kg) mixture and placed in a stereotaxic apparatus (Kopf). Depth of anesthesia was monitored at frequent intervals by tail and toe pinching, and supplemental doses were administered when necessary. Special care was taken to maintain aseptic conditions for the duration of the surgical procedure. Each animal received an injection of pAAV-CaMKIIa-hChR2(H134R)-EYFP (University of North Carolina at Chapel Hill Vector Core) in the right side SpV, using coordinates determined by the Franklin and Paxinos (10) mouse brain atlas (distances are mm from bregma): anteroposterior, –6.5; mediolateral, –1.9; dorsoventral, –5.0. Pressure injections of 250–500 nL of the virus were performed using a 1-μL Hamilton syringe. Following an injection, the needle was left in place for 10–15 min and was retracted 0.7 mm every 10–15 min to minimize the upward suction of the virus. Following the injections, animals were treated locally with lidocaine hydrochloride (Akorn) and vetropolycin antibiotic ointment (Dechra) and were allowed to recover for 14–20 d before they were used in physiological experiments. For the first 36–48 h following surgery, animals received analgesic doses (0.1 mg/kg) of Buprenex (Reckitt Benckiser Healthcare) every 12 h. The virus injections did not produce any observable behavioral or other effects in the animals. Following the survival period, animals were killed and paralemniscal slice preparations were prepared as described above. Patch clamp and voltage clamp mode whole-cell recordings were performed using these slices in the same way as described above. To optogenetically activate the paralemniscal fibers that originate in SpV and terminate in POm, we used a UV laser beam (DPSS Laser). The laser beam had an intensity of 20–80 mW, and each laser illumination lasted 2 ms (355 nm wavelength, frequency-tripled Nd:YVO4, 100 kHz pulse repetition rate). For the assessment of paired-pulse effects, four successive laser illuminations were fired at 10 Hz. Custom-made software written in Matlab (Mathworks) was used to control the laser interface.

Neuroanatomical Techniques. All surgical procedures for the injection of biotinylated dextran amine (BDA) were identical to the ones described above for the injection of AAV. Unilateral injections of 5% BDA (10,000 MW, Molecular Probes) in PBS were iontophoretically delivered (5–12 μA, at 7 s-long on–off cycles, for 15–20 min) using glass pipettes. The injection coordinates were as follows (all distances are from Bregma): S1 injections (anteroposterior, –0.9; mediolateral, –3.0; dorsoventral, –1.5), PrV injections (anteroposterior, –5.0; mediolateral, –1.9; dorsoventral, –4.5), and SpV injections (anteroposterior, –6.5; mediolateral, –1.9; dorsoventral, –5.0). Following surgery, animals were treated locally with lidocaine hydrochloride (Akorn) and ventropolycin antibiotic ointment (Dechra VP). Furthermore, animals were administered buprenex (Reckitt Benckiser Healthcare) every 12 h, for at least 36 h. Following a 72-h survival period, animals were transcardially perfused with PBS followed by 4% paraformaldehyde in PBS. The brains were then placed in an ascending sucrose gradient (10–30%) until saturated. Sections 50 mm thick were cut using a sliding microtome. Alternating slices were used for BDA and Nissl processing. BDA processing was performed as follows: Slices were treated with a 15 min-long wash in 0.5% H_2O_2, three washes in PBS, and a 0.3% Triton-X wash and were finally incubated overnight with ABC reagent (Vectastain ABC-Peroxidase Kit, Vector). Subsequently, after two washes in PBS and two washes in Tris-buffered saline, sections were bathed in diaminobenzidine (DAB, SigmaFast, Sigma-Aldrich) to visualize the label. Finally, sections were mounted onto gelatinized slides, dehydrated, and coverslipped.

Photomicrographs of terminal fields in VPm and POm were taken at 100× with a Retiga 2000 monochrome CCD camera mounted onto a microscope (Leica Microsystems GmbH) and using Q Capture Pro software (QImaging). The resolution of the digital images was 1,600 × 1,200 pixels, and the size of each pixel was 0.075 μm. The plane of focus was determined by the person taking the photos.

The photomicrographs were code-named to avoid bias, and specific patterns of axons and boutons at the edges of a photomicrograph were used as landmarks for transitioning to adjacent areas within the region of interest before the next photomicrograph was taken, thus ensuring that boutons did not appear in more than one photomicrograph. The measurement of the sizes of boutons was done using the AxioVision software (Carl Zeiss Instruments). BDA-labeled boutons were identified by their round shape, and their perimeter was manually marked on a computer screen. Only boutons in the plane of focus (i.e., when there was a clear border between the bouton and the background) were included in the measures. The limits of the resolution at the light microscopic level with our combination of magnification and numerical aperture have been estimated to be around 0.3 μm (11, 12). One thousand boutons were measured in each of the following: in VPm following BDA injections in S1, in VPm following BDA injections in PrV, in POm following BDA injections in S1, and in POm following BDA injections in SpV. Matching nissl-stained sections were used to aid in the identification of boundaries between thalamic nuclei of interest.

Results

A main goal of this study was to test the synaptic properties of the lemniscal inputs to VPm and the paralemniscal inputs to POm. In particular, we sought to determine whether these glutamatergic inputs could be identified as class 1 or class 2, using

previously described criteria (5, 6, 13), or whether some or all of these inputs could be identified as another, heretofore unappreciated type of input. To briefly summarize, class 1 inputs show large initial EPSP amplitudes that tend to be activated in an all-or-none manner and show the property of paired-pulse depression; also, these inputs activate only ionotropic glutamate receptors, mainly AMPA and NMDA. Morphologically, class 1 inputs tend to have relatively large synaptic terminals. Class 2 inputs differ on the above criteria: They show smaller initial EPSPs evoked in a graded manner with paired-pulse facilitation; they activate metabotropic as well as ionotropic glutamate receptors; and they tend to have smaller synaptic terminals.

Viability of Slice Connectivity. During imaging trials using FA, a stimulating electrode was placed on the ML fiber tract, resulting in activation of the lemniscal pathway to VPm (Fig. 1 *A* and *B*). Similarly, to activate the paralemniscal input to POm (Fig. 2*A*), a stimulating electrode was placed on the fibers near the APT, resulting in the activation of POm (Fig. 2*B*). Both VPm and POm activations seen during FA trials could be blocked by the combined application of AP5 and DNQX, which are antagonists to the main ionotropic glutamate receptors.

In experiments involving electrical stimulation, we recorded from a total of 12 VPm cells, which had an uncorrected average membrane potential of –54.7 mV (±6 mV SEM) and an average input resistance of 277 ± 67 MΩ. We also recorded from 39 POm cells with an average uncorrected membrane potential of –57.9 ± 5 mV and an average input resistance of 235 ±85 MΩ.

Electrical Stimulation of Lemniscal and Paralemniscal Inputs.

Lemniscal inputs to VPm. A stimulation of 10 Hz of the lemniscal pathway invariably resulted in the generation of paired-pulse depression (E2/E1 < 1) in the recorded VPm cells. In addition, gradual increases in the stimulation intensity above threshold generally did not result in equivalent increases in response amplitude in the recorded cells; EPSP amplitude remained relatively unaffected by the increase in the amount of current passed through (Fig. 1 *C* and *E*). Lemniscal EPSPs in VPm could be completely blocked by AP5 and DNQX, confirming their glutamatergic nature (Fig. 1*C*, bottom trace). High-frequency stimulation of the lemniscal pathway in the presence of the above-mentioned glutamate receptor antagonists did not produce any membrane potential changes (Fig. 1*D*), reflecting the lack of a metabotropic glutamate receptor activation in this pathway. This pattern of responses (paired-pulse depression, all-or-none responses, and lack of a metabotropic glutamate receptor activation) has previously been described following the stimulation of driver pathways into thalamus (14, 15) but also following the stimulation of some thalamocortical pathways (2, 3, 16, 17). We will refer to these responses as class 1 responses.

Paralemniscal inputs to POm. Stimulation of 10 Hz of the paralemniscal pathway gave raise to two types of EPSPs in POm, which differed on the basis of their short-term plasticity and the relationship between their amplitude and the amount of current used for stimulation. The majority of cells (72%, $n = 28$) manifested paired-pulse facilitation (E2/E1 > 1) (Fig. 2*D*), and the amplitude of the evoked EPSPs had a chiefly monotonic relationship with the amount of stimulation current (Fig. 2*E*, right curves). In addition, in the presence of AP5 and DNQX, these cells responded to high-frequency stimulation with prolonged (>2 s) membrane depolarizations that could be blocked by the mGluR1 receptor antagonist LY367385 (Fig. 2 *D*, *i*). The above pattern of responses (paired-pulse facilitation, graded responses, and activation of metabotropic glutamate receptors) identifies these as class 2 inputs (5, 6, 13).

The remaining POm cells (28%, $n = 11$) responded to paralemniscal stimulation with paired-pulse depression (Fig. 2*C*) and a pattern that resembled the all-or-none response pattern seen in VPm cells after lemniscal stimulation (Fig. 2*E*, left curves). More specifically, for the most part, increases in the stimulus intensity

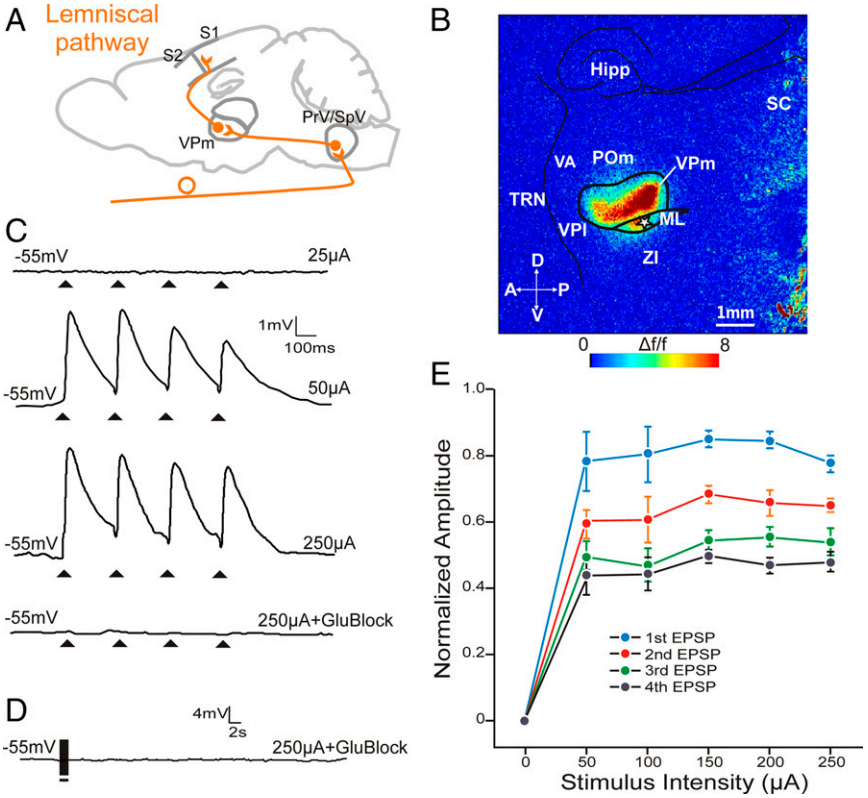

Fig. 1. Electrical stimulation of the lemniscal pathway shows class 1 properties in VPM synapses. (*A*) Schematic of the lemniscal pathway from brainstem PrV/SpV to somatosensory cortex via VPm. (*B*) FA image of a lemniscal brain slice showing activation of VPm in response to electrical stimulation of the ML (white star, 50 μA). No response was observed in surrounding nuclei. (*C*) Example EPSP traces of a VPm cell in response to ML stimulation at subthreshold (25 μA, top trace) and above threshold intensity stimulations (50 μA and 250 μA, second and third traces, respectively). The responses to 250 μA stimulation were abolished with ionotropic glutamate receptor blockers AP5 and DNQX (lower trace). (*D*) High-frequency stimulation of the lemniscal pathway in the presence of AP5 and DNQX did not result in a response, indicating the absence of metabotropic glutamate receptors. (*E*) Normalized EPSP response amplitudes of VPm cells to various stimulation intensities. EPSPs were normalized to the EPSP amplitude that was the highest response at any stimulation intensity within each class. Note the EPSP amplitudes for first > second > third > fourth pulses (paired-pulse depression) for all stimulation intensities. The consistency in amplitude across suprathreshold stimulus intensities illustrates the all-or-none response of this type of synapse. Error bars represent mean ± SEM. Hipp, hippocampus; ML, medial lemniscus; POm, posterior medial nucleus; PrV, principle trigeminal nucleus; SC, superior colliculus; TRN, thalamic reticular nucleus; VA, ventral anterior nucleus; VPl, ventral posterior lateral nucleus; VPm, ventral posterior medial nucleus; ZI, zona incerta.

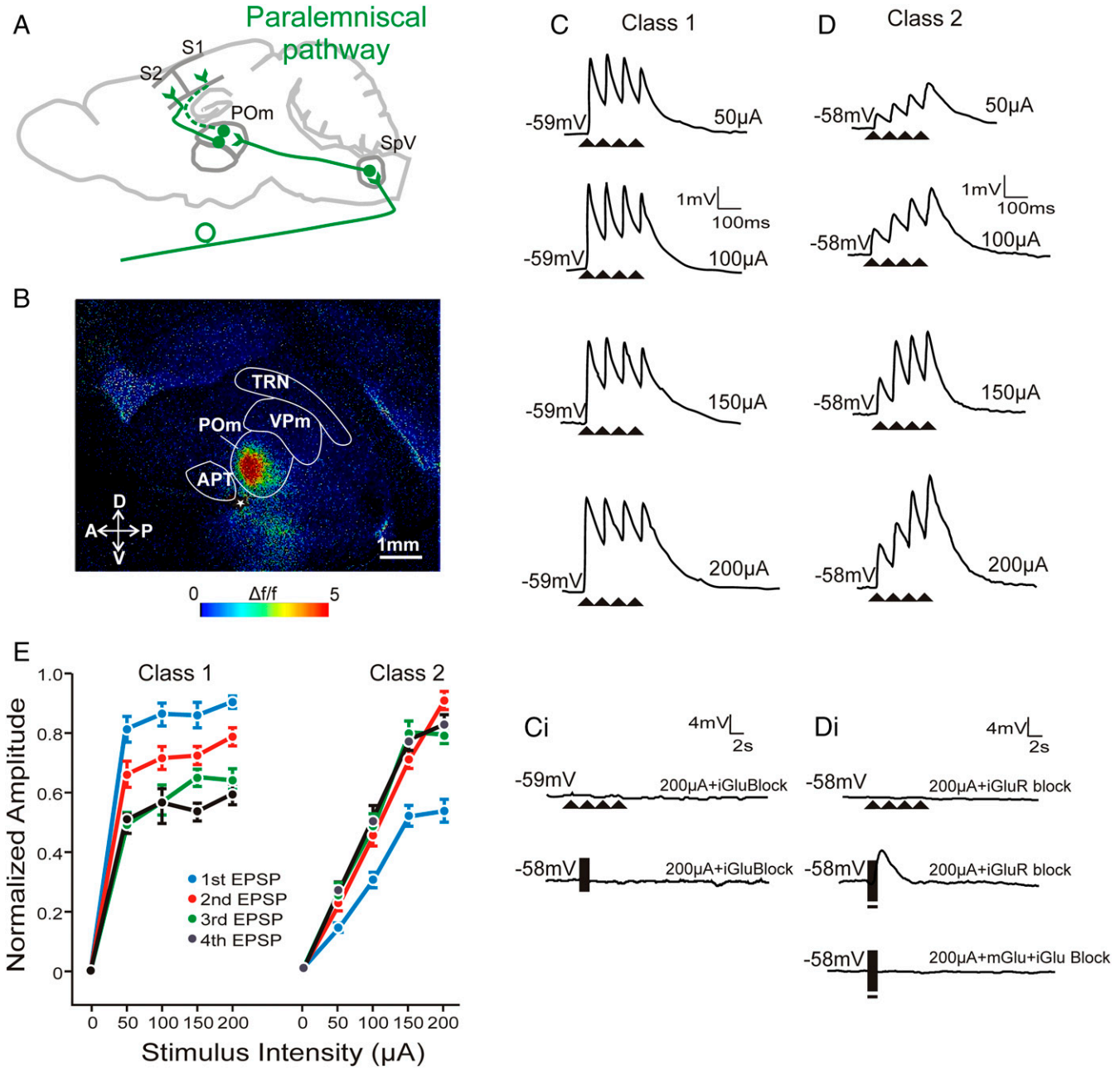

Fig. 2. Electrical stimulation of the paralemniscal pathway shows both class 1 and 2 properties in POm synapses. (*A*) Schematic of the paralemniscal pathway from brainstem SpV to S1 and S2 via POm. (*B*) FA image showing selective activation of POm to electrical stimulation of fibers in the paralemniscal pathway from brainstem (white star, 50 μA). (*C*) Example EPSP traces of a POm cell in response to 10 Hz electrical stimulation at increasing intensities. Paired-pulse depression is observed, a class 1 property. (*C*, *i*) Traces from the same cell during high-intensity stimulation at 10 Hz (upper trace) and high-frequency stimulation (lower trace) in the presence of ionotropic glutamate receptor blockers. (*D*) Example EPSP traces of a POm cell in response to 10 Hz stimulation with paired-pulse facilitation, a class 2 property. (*D*, *i*) Traces from the same cell during high-intensity stimulation at 10 Hz (upper trace) and high-frequency stimulation (middle trace) in the presence of ionotropic glutamate receptor blockers. Note the prolonged membrane depolarization during high-frequency stimulation (middle trace) could be abolished by metabotropic receptor antagonists (bottom trace). (*E*) Normalized EPSP response amplitudes as stimulation intensity increases for both classes. EPSPs were normalized to the EPSP amplitude that was the highest response at any stimulation intensity within each class. In contrast to cells showing a class 1 response ($n = 11$), class 2 cells ($n = 28$) showed EPSP amplitudes that increased dependent on stimulation intensity. Error bars represent mean ± SEM. APT, anterior pretectal nucleus; POm, posterior medial nucleus; SpV, spinal trigeminal nucleus; TRN, thalamic reticular nucleus; VPm, ventral posterior medial nucleus.

did not result in equivalent increases in response amplitude. High-frequency stimulation in the presence of AP5 and DNQX did not evoke a metabotropic glutamatergic, or any other, response in these cells (Fig. 2 *C*, *i*). These paralemniscal responses indicate class 1 inputs and closely resemble those seen in VPm following lemniscal stimulation.

It is worth noting that increasing stimulation intensities did not change the short-term plasticity profiles in any of our cells; that is, a cell responding with paired-pulse depression (or facilitation) to the minimum stimulation intensity would respond with paired-pulse depression (or facilitation) to higher stimulation intensities as well.

At a stimulation intensity of 50 μA (just above threshold stimulation intensity for VPm and POm cells), POm cells that responded with the class 1 pattern produced considerably larger initial EPSPs than did cells with class 2 patterns (4.58 ± 0.30 mV vs. 0.568 ± 0.035 mV; $P < 0.001$ on a Mann–Whitney U test), but these first EPSP amplitudes for the POm cells showing class 1 input were very similar to those produced by lemniscal stimulation in VPm cells (4.57 ± 0.54 mV vs. 4.58 ± 0.30 mV; $P > 0.1$ on a Mann–Whitney U test).

Optogenetic Activation of SpV Inputs to POm. Whereas the electrical stimulation of glutamatergic inputs to POm likely reflect input from the spinal cord or SpV, other possibilities for the input origin might exist, and so we wanted to verify that the pattern seen with electrical activation could be reproduced with optogenetic activation of axons known to originate in SpV. The paralemniscal slices that were prepared from the brains of animals injected with AAV into SpV expressed ChR-YFP throughout POm and VPm (Fig. 3*A*). The brainstem of these brains was sliced separately in the coronal plane to examine the extent and accuracy of the injection site (Fig. 3 *A*, *i*). Animals with injections that missed SpV are not considered further. Single-pulse photostimulation at various locations near a recorded POm cell produced EPSCs. One or more of these locations were then selected for the delivery of four laser pulses (10 Hz) to examine the paired-pulse effects of the pathway. Similarly to what we saw following the electrical stimulation of the paralemniscal pathway, we identified two different patterns of responses in POm cells following photoactivation of the paralemniscal fibers. The majority of cells (71%, $n = 12$) responded to repetitive photostimulation with paired-pulse facilitation (Fig. 3*B*, lower trace), whereas the remaining cells (29%, $n = 5$) responded with paired-pulse depression (Fig. 3*C*, lower trace). Whenever possible we placed a stimulating electrode on the slice (as described in *Methods*) and examined the paired-pulse effects with electrical stimulation of the paralemniscal pathway. We managed this for two cells showing class 1 inputs and five showing class 2. For every one of these cells, we saw the same activation pattern, including response amplitudes and paired-pulse depression or facilitation with electrical stimulation as we did with photostimulation (upper traces in Fig. 3 *B* and *C*).

The high-stimulation frequencies required for the reliable activation of metabotropic glutamate receptors (>125 Hz) are a challenge for photostimulation due to the kinetics of currently available opsins (18). We therefore tested for the activation of these receptors with electrical high-frequency stimulation in the presence of AP5 and DNQX (as described in *Methods*). Cells that responded to optogenetic paralemniscal stimulation with paired-pulse facilitation responded to electrical high-frequency stimulation with a prolonged depolarization (Fig. 3 *B*, *i*) that could be blocked by LY367385. On the other hand, cells that responded to optogenetic stimulation with paired-pulse depression did not show any signs of metabotropic glutamatergic activation (Fig. 3 *C*, *i*).

Electrical and Optogenetic Classifications of Class 1 and Class 2 Cells. The data obtained through optogenetic photostimulation of the paralemniscal pathway to POm was highly comparable with data obtained through electrical stimulation of the same pathway. This is well illustrated in the paired-pulse ratio (second EPSP/first EPSP), which distinguishes class 2 (ratio >1) from class 1 (ratio <1) responses. These ratios were similar for class 1 POm cells using electrical and optogenetic stimulation (electrical vs. optogenetic, 0.81 ± 0.042 vs. 0.72 ± 0.047, $P > 0.99$, Kruskal–Wallis test) and class 2 POm cells (electrical vs. optogenetic, 1.89 ± 0.13 vs. 1.69 ± 0.14, $P > 0.99$, Kruskal–Wallis test) (Fig. 4*A*). E2/E1 ratios also show a similarity between class 1 responses in VPm and POm, whether using electrical (VPm class 1 vs. POm class 1 electrical, 0.79 ± 0.05 vs. 0.81 ± 0.042, $P > 0.99$, Kruskal–Wallis test) or optogenetic stimulation (VPm class 1 vs. POm class 1 optogenetic, 0.79 ± 0.05 vs. 0.72 ± 0.05, $P > 0.99$, Kruskal–Wallis test). Furthermore, the proportions of class 2 cells classified using electrical stimulation (72%, $n = 28$ of 39) were similar to the proportions classified using optogenetic stimulation (71%, $n = 12$ of 17). Overall, using either stimulation technique to activate the paralemniscal pathway, we report 71% of recorded POm cells responded with class 2 properties and 29% responded with class 1 properties ($n = 56$) (Fig. 4 *A*, *i*).

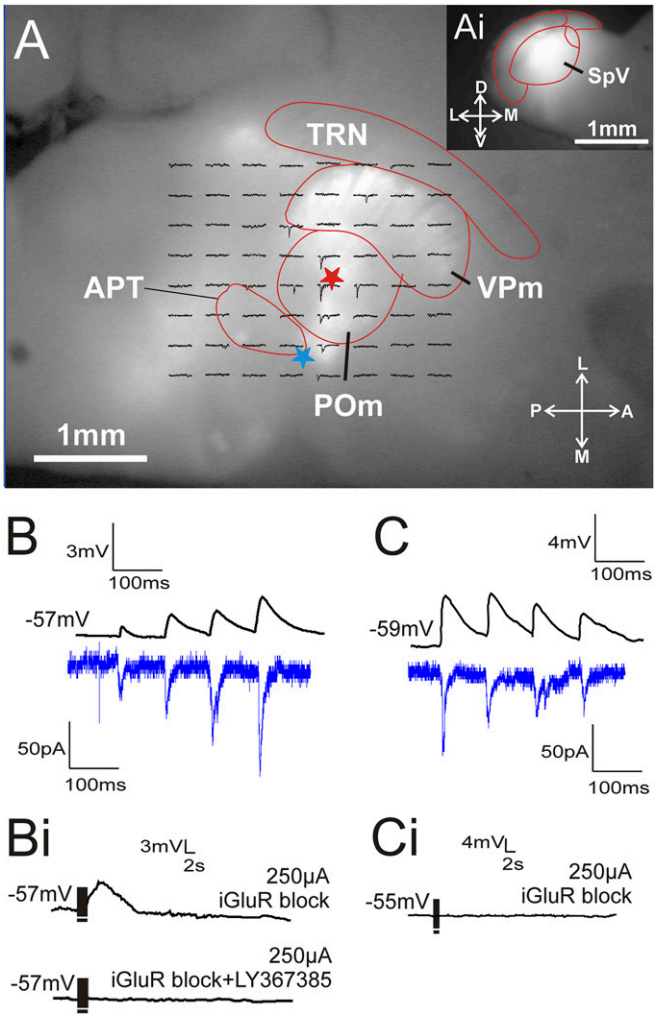

Fig. 3. Optogenetic stimulation of the paralemniscal pathway in POm. (*A*) Image of a paralemniscal slice during recording shows ChR2-eYFP expression in POm and VPm after SpV injection (shown in *A*, *i*). A grid is overlaid on the patched POm cell (red star) where traces on the grid represent the single-pulse EPSC response of the POm cell to focal laser stimulation at that particular position. An electrode was also placed on fibers of the paralemniscal pathway (blue star) to compare optogenetic and electrical stimulation responses. (*B*) Example traces showing that a cell with class 2 paired-pulse facilitation responses to laser activation (bottom trace) also responded to electrical stimulation (top trace) in the same manner. (*B*, *i*) The same example cell in response to high-frequency electrical stimulation in the presence of ionotropic glutamate receptor blockers (upper trace) and in the presence of ionotropic and metabotropic glutamate receptor blockers (lower trace). (*C*) Example traces of a POm cell responding with the class 1 property of paired-pulse depression after both electrical stimulation (top trace) and optogenetic stimulation (bottom trace). (*C*, *i*) Responses from the same cell were blocked by ionotropic glutamate receptor antagonists during high-frequency electrical stimulation. APT, anterior pretectal nucleus; POm, posterior medial nucleus; SpV, spinal trigeminal nucleus; TRN, thalamic reticular nucleus; VPm, ventral posterior medial nucleus.

Similarities Between POm Cells with Class 1 and Class 2 Responses. We attempted to find other properties that would further delineate the two distinct classes of glutamatergic POm cells we report here. Cells with class 1 ($n = 16$) and class 2 ($n = 40$) responses in POm did not differ with respect to their resting membrane potential (Mann–Whitney, $P > 0.05$) or their input resistance (Mann–Whitney, $P > 0.05$).

Reports from the rat (19) suggest that POm contains two populations of cells that respond differently to the application of cholinergic agonists. More specifically, although the majority of cells (75–80%) respond to Acetyl-β-methylcholine (MCh) with membrane depolarization, a considerable minority (20–25%) respond with membrane hyperpolarization. These proportions resemble the proportions of POm cells with class 1 and class 2 responses in our data, and we thus wanted to test if there was a relationship between the response of POm cells to paralemniscal stimulation (class 1 or class 2) and to the acetylcholine agonist MCh (200–250 μM; Sigma-Aldrich). This was bath applied for 30 s, and membrane potential was recorded for 5–10 additional minutes, which was typically enough time for the membrane potential to return to preapplication baseline levels. This was done in the presence of low-Ca^{2+} (0.5 mM) and high-Mg^{2+} (8 mM) ACSF to block synaptic transmission and ensure that the responses seen were postsynaptic to the recorded cell. All POm cells that were tested (class 1, $n = 14$; class 2, $n = 7$) responded to MCh application with membrane depolarization, thus providing no further basis for differentiation between the two types of cells.

The two populations of cells within POm that we identified were also compared with regard to their spike frequency adaptation (SFA) patterns. After patching onto a cell and before any agonists or antagonists were introduced to the bath, 1 s-long current injection pulses (250, 400, or 700 pA) were applied to induce spiking. When necessary, cells were depolarized and held at –50 mV to inactivate the low threshold T current (20) and thus prevent burst firing. An SFA index was calculated as follows:

$$\text{Spike Frequency Adaptation Index} = (\text{First } \tau - \text{Last } \tau)/\text{First } \tau,$$

where τ = interspike interval.

All cells of both classes responded with adapting spiking patterns, especially for the highest current intensities (Mann–Whitney, $P > 0.05$ for all current injection intensities).

Finally, based on photographs taken during electrophysiological recordings, the relative locations of cells of the two response classes were charted onto POm, but no location trends were observed for either cell type (Fig. 4*B*).

Bouton Sizes. In addition to the electrophysiological properties of the lemniscal and paralemniscal inputs into thalamus, we also wanted to examine some anatomical features of these pathways. Inputs with driver or class 1 properties have been associated with both small and large terminal boutons, whereas inputs with modulatory or class 2 properties have been associated with small terminal boutons only (2, 3, 21). We injected SpV and PrV with BDA and examined the sizes of terminal boutons in POm and VPm, respectively. We also examined the size of terminal boutons in these two thalamic nuclei following injections of BDA in S1. We already know that layer 5 of S1 provides POm with driving (class 1) input, whereas layer 6 of S1 provides VPm with modulatory (class 2) input (15). As a result, the size of terminal boutons in these two thalamic nuclei following BDA injections in S1 would provide us with a direct comparison with regard to the size of boutons expected from pathways responsible for class 1 versus class 2 responses.

BDA injections in S1, SpV, and PrV produced anterograde labeling within VPm and POm (Fig. 5 *A*–*G*). The average size of boutons in POm following injections in SpV (0.91 $\mu m^2 \pm$ 0.02 SEM) was significantly smaller than the average size of boutons in VPm following injections of BDA in PrV (2.28 $\pm$ 0.06 μm^2, Mann–Whitney, $P < 0.0001$) and also smaller than the size of boutons in POm following BDA injections in S1 (1.25 $\pm$ 0.027 μm^2, Mann–Whitney, $P < 0.0001$). Finally the size of boutons in VPm following injections of BDA in PrV was significantly larger than those in VPm following injections of BDA in S1 (0.78 $\pm$ 0.01 μm^2, Mann–Whitney, $P < 0.0001$) (Fig. 5*H*). The largest boutons are those associated with a purely class 1 input (PrV to VPm), the smallest with a purely class 2 input (S1 layer 6 to VPm), and intermediate sizes with mixed class 1 and 2 inputs (SpV to POm and S1 to POm, which

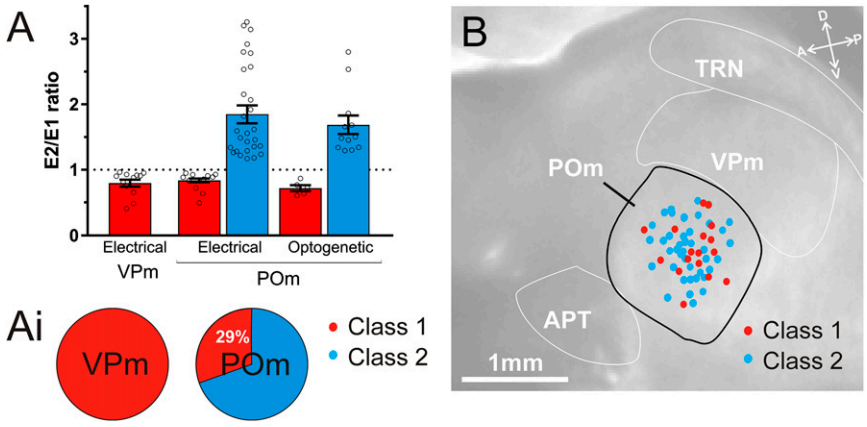

Fig. 4. Summary of class 1 and class 2 responses to lemniscal and paralemniscal inputs to VPm and POm using electrical and optogenetic stimulation. (*A*) The E2/E1 ratios (second pulse amplitude/first pulse amplitude) of all recorded cells in response to 10 Hz stimulation of the lemniscal pathway to VPm ($n = 12$, tested electrically) and the paralemniscal pathway to POm ($n = 39$ tested electrically and $n = 17$ optogenetically). Paired-pulse depression (E2/E1 ratio <1) indicates a synapse has class 1 properties (red bars), and paired-pulse facilitation (ratio >1) indicates a synapse has class 2 properties (blue bars). Note the consistency of ratios for each class across nuclei and stimulation technique. (*A*, *i*) Proportions of class 1 and class 2 cells in VPm ($n = 12$) and POm ($n = 56$). In the case of POm, these proportions represent the combination of electrical and optogenetic experiments. (*B*) Locations of recorded POm cells classified as class 1 and class 2. Locations were reconstructed from photos taken during electrical and optogenetic stimulation recordings and superimposed on a representative image of the paralemniscal slice. The positions of cells classified as class 1 (red dots, $n = 16$) and class 2 (blue dots, $n = 40$) did not show obvious location trends. Error bars represent mean $\pm$ SEM. APT, anterior pretectal nucleus; POm, posterior medial nucleus; TRN, thalamic reticular nucleus; VPm, ventral posterior medial nucleus.

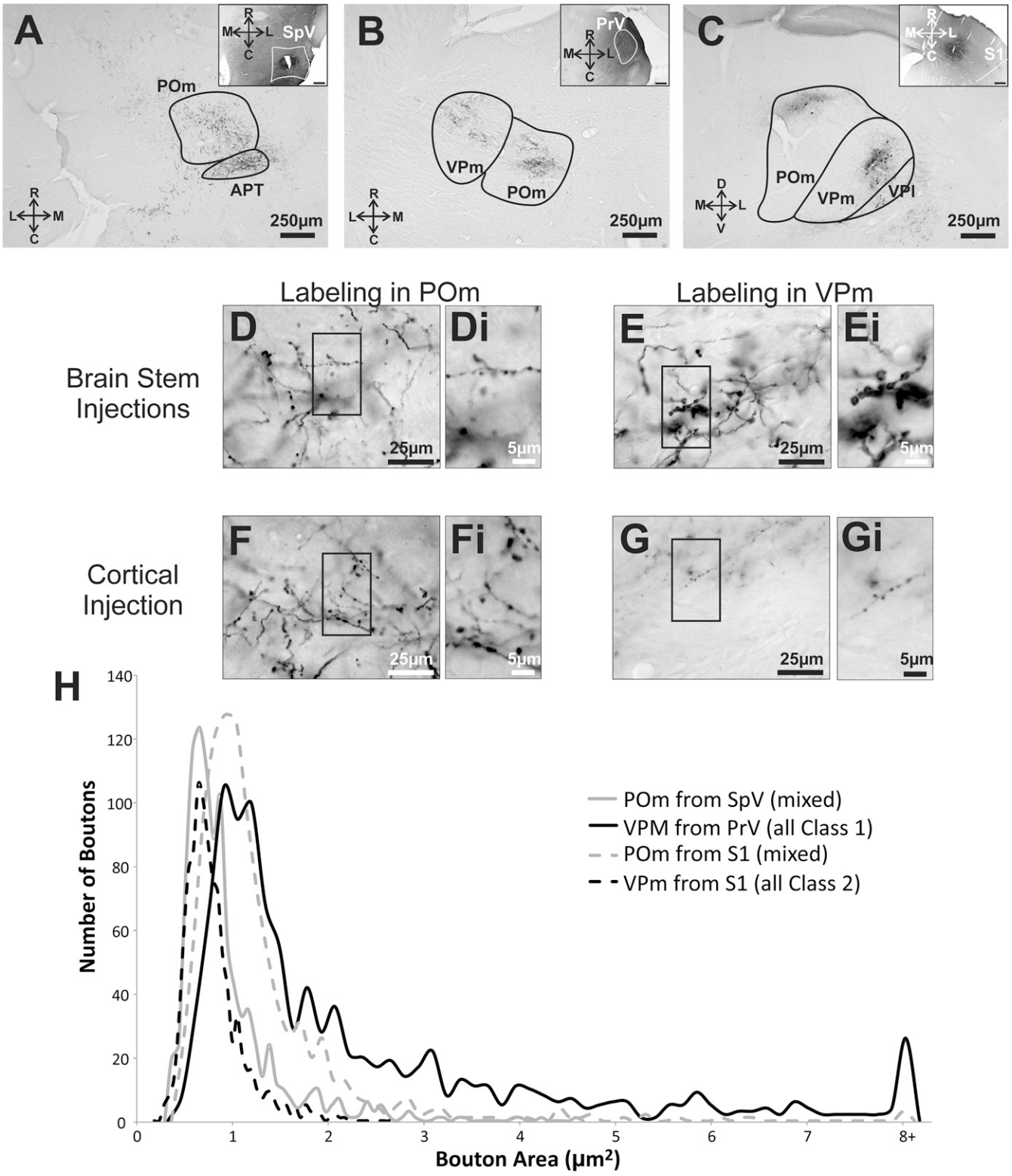

Fig. 5. Terminal bouton size measurements in thalamus from cortical and brainstem structures. Example photos showing BDA anterograde labeling in thalamus from (*A*) SpV injection, (*B*) PrV injection, and (*C*) S1 injection. The corresponding *Insets* show the injection sites. Note that PrV injections likely included surrounding brainstem structures that also project to POm. Enlarged images of BDA-labeled synaptic terminals in (*D*) POm from SpV, (*E*) VPm from PrV, (*F*) POm from S1, and (*G*) VPm from S1. *D*, *i*–*G*, *i* are further enlargements of boxes in *D*–*G*. (*H*) Bouton size for each projection shows, in general, that the synaptic boutons of class 1 projections are larger than that of class 2 boutons.

contains both class 2 layer 6 and class 1 layer 5 components). This pattern is consistent with earlier evidence that class 1 inputs terminate in larger boutons on average than do class 2 inputs (reviewed in refs. 4–6).

Discussion

It is of obvious importance to understand the functional organization of routes used by sensory pathways to bring information to the cortex. In the case of somatosensory pathways, there are two main routes that have been anatomically defined: a lemniscal route with a thalamic relay via VPm and a paralemniscal route relayed via POm. The issue raised here relates to the synaptic properties of the lemniscal and paralemniscal connections to their target thalamic relay cells in the mouse. Whereas the synapses involved are all glutamatergic, they are not functionally homogeneous: Indeed, we found that those of the lemniscal pathway are all class 1 but that most of the paralemniscal inputs are class 2, with the remainder being class 1. This finding is consistent with the lemniscal pathway representing an information route to cortex but it also raises doubts as to whether the paralemniscal pathway represents a parallel information route.

Our evidence that lemniscal inputs to VPm relay cells is based on criteria developed for other thalamic and cortical circuits and involves such parameters as relatively large initial EPSP amplitudes, synaptic paired-pulse depression, an all-or-none activation pattern, activation of ionotropic but not metabotropic glutamate receptors, and the morphological feature of relatively large synaptic terminals (reviewed in refs. 4–6, 22). These findings are in line with previous reports for these synapses of all-or-none glutamatergic-dependent paired-pulse depression (23). Likewise, our evidence of mostly class 2 inputs to POm relay cells via the paralemniscal route is based on multiple criteria, including relatively small initial EPSP amplitudes, synaptic paired-pulse facilitation, a graded activation pattern, activation of both ionotropic and metabotropic receptors, and the morphological feature of relatively small synaptic terminals (reviewed in refs. 4–6). These class 1 and class 2 properties are virtually the same as has been described for other thalamic and cortical pathways (2, 3, 14–17, 24–27).

Technical Issues and Provisos. One question that arises is the identity of inputs that we activated electrically. In the case of the lemniscal inputs to VPm, we clearly identified the ML for stimulation, and so by definition, we activated the lemniscal input. However, we cannot be certain of the source of the activated axons: They likely included inputs from both PrV and SpV. Nonetheless, the observation that such activation always evoked class 1 inputs makes this distinction moot.

The situation for electrical activation of the paralemniscal input is less clear, because there is no readily identifiable pathway for activation. One special concern is that, instead of brainstem glutamatergic axons, we activated branches of cortical layer 5 axons that innervated POm. However, this seems unlikely (although not impossible) as explained in *Methods*. In any case, it is precisely because of these uncertainties that we used optogenetics, the results of which indicate that paralemniscal inputs from SpV to POm show the same mix of class 1 and class 2 inputs as seen with electrical activation. For these reasons, we feel that our conclusion that most paralemniscal inputs to POm are class 2, with the remainder being class 1, is justified.

Finally, we have interpreted the EPSPs we evoked as monosynaptic for the following reasons. Mainly, a polysynaptic glutamatergic response would have to involve local circuitry in thalamus, which is almost completely GABAergic and, in the cases of VPm and POm, derives almost exclusively from the thalamic reticular nucleus (see ref. 28). Thus, there is no neuronal substrate for evoking local glutamatergic inputs from activation of distant inputs to POm, as we have done. The only reasonable interpretation of the evoked EPSPs is that they are monosynaptic. It is noteworthy that the latency and consistency of amplitude and latency in evoked EPSPs is also in agreement with monosynaptic innervation.

Significance of the Class 1 and 2 Input Patterns. We have argued elsewhere that class 1 and 2 glutamatergic inputs serve different roles in excitatory transmission (5, 6). For class 1 synapses, the large, depressing EPSPs reflect a high probability of transmitter release, features that support reliable transmission of information. We have also argued that class 2 inputs, which act via metabotropic glutamate receptors, are ill-suited for the basic transmission of information due to their smaller initial EPSPs, lower probability of transmitter release, and graded activation pattern. Regarding EPSP amplitudes, an important parameter is that of the initial EPSP in a train (see Fig. 2 *C* and *D*), because large initial EPSPs are required for efficient information transfer. Class 1 inputs generally evoke much larger initial EPSPs than class 2 inputs do. Indeed, class 2 EPSPs typically begin to approach the sizes of class 1 only under one of two conditions. One is if many individual afferents are synchronously activated by a high-amplitude current, which seems nonphysiological, or late in the train in situations of synaptic facilitation, which would mean such large EPSPs would occur late in a response, a situation poorly designed for temporally precise information transfer.

We suggest that class 2 inputs instead mainly serve a modulatory function. Examples of such modulation by class 2 inputs include control of tonic versus burst firing mode of thalamic relay cells (29, 30) and affecting the EPSP amplitudes of class 1 inputs (1, 31–35). Also consistent with this modulatory role for class 2 inputs are in vivo studies showing that optogenetic manipulation of the class 2 corticogeniculate pathway from cortical layer 6 shows that gain control is one of its main roles (36, 37). The effect of class 2 inputs, whether inhibition or excitation, did not alter the orientation tuning of the postsynaptic cells in these studies. In contrast, manipulating class 1 inputs, such as from retina to the lateral geniculate nucleus or from the lateral geniculate nucleus to visual cortex, severely disrupts receptive field properties (38, 39).

For the above reasons, class 1 and 2 inputs have also been, respectively, referred to as "driver" and "modulator" (5, 6). It should be noted, however, that this terminology does not mean that class 2 inputs carry no information content. Their modulatory function reflects actions based on information that class 2 afferents represent in the same way that the classical modulators (e.g., cholinergic or serotonergic) do. In this regard, our finding that lemniscal inputs to VPm relay cells are class 1 is entirely consistent with this projection representing part of a main information route to cortex. Indeed, the lemniscal pathway faithfully carries the somatosensory receptive field properties from periphery through VPm to S1 (40–42). However, our finding that most POm relay cells receive class 2 input from a source that is mostly if not exclusively from SpV raises questions regarding the functional significance of the paralemniscal pathway.

Significance of Paralemniscal Inputs to POm. Fig. 6*A* shows the conventional view that the lemniscal and paralemniscal pathways represent two parallel information streams to cortex. However, because the majority of POm relay cells receive paralemniscal input that may be regarded as modulatory, it follows that the main source of information relayed by these cells plausibly derives from another neuronal site. It is relevant in this context that an important difference has been described for the hierarchical relationship between VPm and POm. VPm is defined as a *first order* thalamic relay because it receives its class 1, or driver, input from subcortical sources, namely PrV and SpV, whereas POm is defined as a *higher order* thalamic relay because many, most, or all POm relay cells are driven by layer 5 of another cortical area. Thus, higher order relays are seen as a central element in transthalamic circuits between cortical areas (4–6). For instance, one such circuit has been defined from layer 5 of S1 via POm to S2 (43).

Fig. 6 *B–F* shows several possibilities of the circuits entered into by paralemniscal input to POm. One possibility is that the majority of paralemniscal inputs to POm cells act to modulate

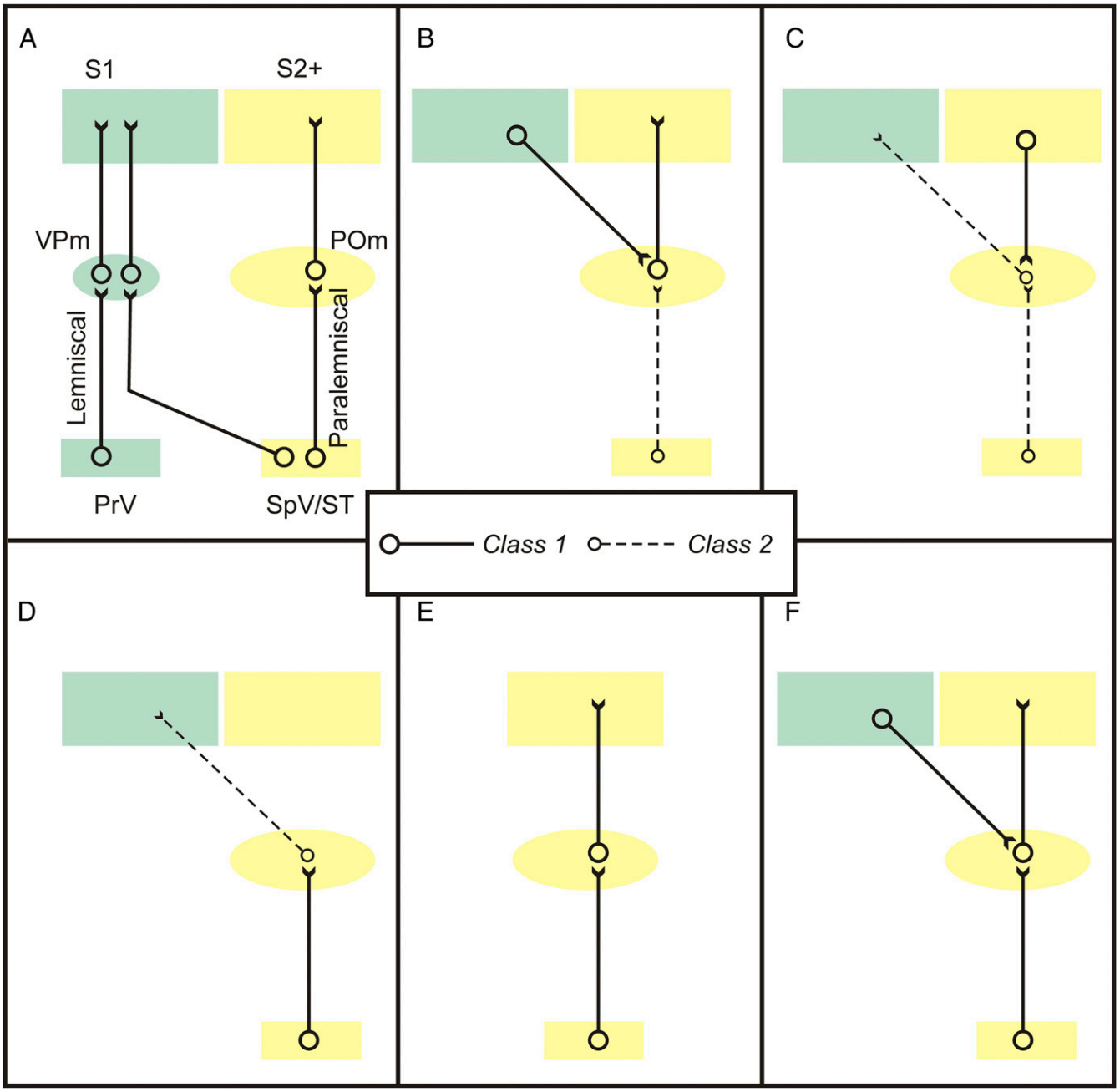

Fig. 6. Possible circuit organizations of lemniscal and paralemniscal pathways. A common hypothesis is that class 1 (driver) inputs (solid black lines) are information-bearing and class 2 (modulator) inputs (dotted black lines) modulate; see text for details. (*A*) Conventional view; the pathways form parallel information streams through thalamus to cortex. This is challenged due to our observation that most paralemniscal inputs to POm are class 2. (*B* and *C*) Possible functions of class 2 paralemniscal inputs to POm. These are not mutually exclusive and do not exhaust possibilities. (*B*) These modulate the transthalamic pathway from S1 to S2 and possibly other areas. (*C*) These modulate a feedback transthalamic modulatory circuit from S2 and possibly other areas to S1. (*D–F*) Possible functions of class 1 paralemniscal inputs to POm. (*D*) These drive a modulator input to S1. (*E*) These drive an information route to S2 and possibly other areas. (*F*) These converge with other driver inputs to POm cells, such as from S1. POm, posterior medial nucleus, PrV, principal and spinal nuclei of the Vth nerve; S1, primary somatosensory cortex; S2+, secondary somatosensory cortex plus other cortical targets of POm (e.g., higher order somatosensory areas or primary motor cortex); SpV/ST, spinal trigeminal nucleus plus spinothalamic tract; VPm, ventral posterior medial nucleus.

this transthalamic circuit (Fig. 6*B*). It has also been shown that the input from POm to S1 is entirely class 2 or modulatory (2). If the paralemniscal input to these POm cells is class 2, then this would likely modulate whatever drives these cells (e.g., layer 5 of S2; Fig. 6*C*); if instead the paralemniscal class 1 or driver input to POm innervates these cells, then this would represent a circuit that acts to modulate S1 (Fig. 6*D*). Neither of these possibilities is compatible with the idea that the paralemniscal pathway represents a parallel, main information route to cortex. Of course, it is also possible that some or all of the class 1 paralemniscal input to POm innervates relay cells projecting to S2, which would represent such a parallel information route (Fig. 6*E*). It is also possible that class 1 paralemniscal input to POm converges onto cells that also receive a class 1 input from layer 5 of S1 (Fig. 6*F*), and there is support for this (44). Other possibilities also exist, and it is thus clear that more detailed circuit analysis is needed regarding the

paralemniscal input to POm relay cells to understand the role this pathway plays in somatosensation.

Comparison of Somatosensory and Auditory Inputs to Thalamus. We have shown that the majority (71%) of paralemniscal inputs to POm appear to have a modulatory function, and as discussed in the preceding paragraph, those inputs that are class 1 (driver) may actually contribute to a circuit that does not "drive" information all of the way to cortex, because this class 1 input might contact POm cells that provide class 2 input to S1 (2). These points raise doubts about the notion that the paralemniscal pathway to cortex offers a parallel information channel much like the lemniscal one and may instead play a mostly modifying role in relaying somatosensory signals to cortex. This is interesting in the context that a similar analysis of the inputs to auditory thalamus may be organized in an analogous fashion. The ventral division of the medial geniculate nucleus (MGNv) is first order, analogous to VPm, and the dorsal division (MGNd) is higher order, analogous to POm. The projection from the core region of the inferior colliculus to MGNv is analogous to the lemniscal input to VPm, and the projection from the shell region of the inferior colliculus to MGNd is analogous to the paralemniscal input. These had been viewed as parallel information routes to auditory cortex, but an analysis of the synaptic properties of the inputs to the MGN demonstrated that MGNv relay cells received only class 1, or driver, input from the collicular core region and that MGNd relay cells received only class 2, or modulator, input from the collicular shell region (26). Thus, the paralemniscal pathway in this case seems to play a modulatory role and not one as the main information-bearing input.

Conclusions

Our data reveal the dual nature of the glutamatergic paralemniscal pathway primarily as a modulator of POm projections but also partially as an information route to POm. To fully understand the role of these paralemniscal inputs to thalamus requires more information about the projections of the targeted POm cells. Rather than simply representing an alternate version of the lemniscal pathway for encoding information, the paralemniscal pathway seems to be involved largely if not completely in modulating somatosensory information processed by thalamocortical circuits.

ACKNOWLEDGMENTS. This work was supported by National Institute of Neurological Disorders and Stroke Grant NS094184 and National Eye Institute Grant EY022338 (both to S.M.S.). C.M. was supported by National Health and Medical Research Council (Australia) CJ Martin Fellowship 1106370.

1. Liu T, Petrof I, Sherman SM (2015) Modulatory effects of activation of metabotropic glutamate receptors on GABAergic circuits in the mouse thalamus. *J Neurophysiol* 113:2646–2652.
2. Viaene AN, Petrof I, Sherman SM (2011) Properties of the thalamic projection from the posterior medial nucleus to primary and secondary somatosensory cortices in the mouse. *Proc Natl Acad Sci USA* 108:18156–18161.
3. Viaene AN, Petrof I, Sherman SM (2011) Synaptic properties of thalamic input to layers 2/3 and 4 of primary somatosensory and auditory cortices. *J Neurophysiol* 105: 279–292.
4. Sherman SM (2016) Thalamus plays a central role in ongoing cortical functioning. *Nat Neurosci* 19:533–541.
5. Sherman SM, Guillery RW (2013) *Thalamocortical Processing: Understanding the Messages That Link the Cortex to the World* (MIT Press, Cambridge, MA).
6. Sherman SM, Guillery RW (1998) On the actions that one nerve cell can have on another: Distinguishing "drivers" from "modulators". *Proc Natl Acad Sci USA* 95: 7121–7126.
7. Veinante P, Lavallée P, Deschênes M (2000) Corticothalamic projections from layer 5 of the vibrissal barrel cortex in the rat. *J Comp Neurol* 424:197–204.
8. Llano DA, Theyel BB, Mallik AK, Sherman SM, Issa NP (2009) Rapid and sensitive mapping of long-range connections in vitro using flavoprotein autofluorescence imaging combined with laser photostimulation. *J Neurophysiol* 101:3325–3340.
9. Shibuki K, et al. (2003) Dynamic imaging of somatosensory cortical activity in the rat visualized by flavoprotein autofluorescence. *J Physiol* 549:919–927.
10. Paxinos G, Franklin KBJ (2008) *The Mouse Brain in Stereotaxic Coordinates* (Academic, London).
11. Llano DA, Sherman SM (2008) Evidence for nonreciprocal organization of the mouse auditory thalamocortical-corticothalamic projection systems. *J Comp Neurol* 507: 1209–1227.
12. Friedlander MJ, Lin C-S, Stanford LR, Sherman SM (1981) Morphology of functionally identified neurons in lateral geniculate nucleus of the cat. *J Neurophysiol* 46:80–129.
13. Guillery RW, Sherman SM (2002) Thalamic relay functions and their role in corticocortical communication: Generalizations from the visual system. *Neuron* 33:163–175.
14. Petrof I, Sherman SM (2009) Synaptic properties of the mammillary and cortical afferents to the anterodorsal thalamic nucleus in the mouse. *J Neurosci* 29:7815–7819.
15. Reichova I, Sherman SM (2004) Somatosensory corticothalamic projections: Distinguishing drivers from modulators. *J Neurophysiol* 92:2185–2197.
16. Viaene AN, Petrof I, Sherman SM (2011) Synaptic properties of thalamic input to the subgranular layers of primary somatosensory and auditory cortices in the mouse. *J Neurosci* 31:12738–12747.
17. Lee CC, Sherman SM (2008) Synaptic properties of thalamic and intracortical inputs to layer 4 of the first- and higher-order cortical areas in the auditory and somatosensory systems. *J Neurophysiol* 100:317–326.
18. Gunaydin LA, et al. (2010) Ultrafast optogenetic control. *Nat Neurosci* 13:387–392.
19. Varela C, Sherman SM (2007) Differences in response to muscarinic agonists between first and higher order thalamic relays. *J Neurophysiol* 98:3538–3547.
20. Jahnsen H, Llinás R (1984) Electrophysiological properties of guinea-pig thalamic neurones: An *in vitro* study. *J Physiol* 349:205–226.
21. Li J, Guido W, Bickford ME (2003) Two distinct types of corticothalamic EPSPs and their contribution to short-term synaptic plasticity. *J Neurophysiol* 90:3429–3440.
22. Petrof I, Sherman SM (2013) Functional significance of synaptic terminal size in glutamatergic sensory pathways in thalamus and cortex. *J Physiol* 591:3125–3131.
23. Castro-Alamancos MA (2002) Properties of primary sensory (lemniscal) synapses in the ventrobasal thalamus and the relay of high-frequency sensory inputs. *J Neurophysiol* 87:946–953.
24. Covic EN, Sherman SM (2011) Synaptic properties of connections between the primary and secondary auditory cortices in mice. *Cereb Cortex* 21:2425–2441.
25. De Pasquale R, Sherman SM (2011) Synaptic properties of corticocortical connections between the primary and secondary visual cortical areas in the mouse. *J Neurosci* 31: 16494–16506.
26. Lee CC, Sherman SM (2010) Topography and physiology of ascending streams in the auditory tectothalamic pathway. *Proc Natl Acad Sci USA* 107:372–377.
27. Lee CC, Sherman SM (2009) Modulator property of the intrinsic cortical projection from layer 6 to layer 4. *Front Syst Neurosci* 3:3.
28. Arcelli P, Frassoni C, Regondi MC, De Biasi S, Spreafico R (1997) GABAergic neurons in mammalian thalamus: A marker of thalamic complexity? *Brain Res Bull* 42:27–37.
29. Godwin DW, Vaughan JW, Sherman SM (1996) Metabotropic glutamate receptors switch visual response mode of lateral geniculate nucleus cells from burst to tonic. *J Neurophysiol* 76:1800–1816.
30. Wang W, Jones HE, Andolina IM, Salt TE, Sillito AM (2006) Functional alignment of feedback effects from visual cortex to thalamus. *Nat Neurosci* 9:1330–1336.
31. Liu T, Petrof I, Sherman SM (2014) Modulatory effects of activation of metabotropic glutamate receptors on GABAergic circuits in the mouse cortex. *J Neurophysiol* 111: 2287–2297.
32. De Pasquale R, Sherman SM (2013) A modulatory effect of the feedback from higher visual areas to V1 in the mouse. *J Neurophysiol* 109:2618–2631.
33. Lam YW, Sherman SM (2013) Activation of both Group I and Group II metabotropic glutamatergic receptors suppress retinogeniculate transmission. *Neuroscience* 242: 78–84.
34. De Pasquale R, Sherman SM (2012) Modulatory effects of metabotropic glutamate receptors on local cortical circuits. *J Neurosci* 32:7364–7372.
35. Lee CC, Sherman SM (2009) Glutamatergic inhibition in sensory neocortex. *Cereb Cortex* 19:2281–2289.
36. Olsen SR, Bortone DS, Adesnik H, Scanziani M (2012) Gain control by layer six in cortical circuits of vision. *Nature* 483:47–52.
37. Denman DJ, Contreras D (2015) Complex effects on in vivo visual responses by specific projections from mouse cortical layer 6 to dorsal lateral geniculate nucleus. *J Neurosci* 35:9265–9280.
38. Ferster D, Chung S, Wheat H (1996) Orientation selectivity of thalamic input to simple cells of cat visual cortex. *Nature* 380:249–252.
39. Hubel DH, Wiesel TN (1961) Integrative action in the cat's lateral geniculate body. *J Physiol* 155:385–398.
40. Brecht M, Sakmann B (2002) Whisker maps of neuronal subclasses of the rat ventral posterior medial thalamus, identified by whole-cell voltage recording and morphological reconstruction. *J Physiol* 538:495–515.
41. Friedberg MH, Lee SM, Ebner FF (1999) Modulation of receptive field properties of thalamic somatosensory neurons by the depth of anesthesia. *J Neurophysiol* 81: 2243–2252.
42. Simons DJ, Carvell GE (1989) Thalamocortical response transformation in the rat vibrissa/barrel system. *J Neurophysiol* 61:311–330.
43. Theyel BB, Llano DA, Sherman SM (2010) The corticothalamocortical circuit drives higher-order cortex in the mouse. *Nat Neurosci* 13:84–88.
44. Groh A, et al. (2014) Convergence of cortical and sensory driver inputs on single thalamocortical cells. *Cereb Cortex* 24:3167–3179.